Mapping Cretaceous faults using a convolutional neural network

– A field example from the Danish North Sea

MADS C. L. LORENTZEN[1, 3, *], KENNETH BREDESEN[1], FLORIAN W. H. SMIT[1], TORSTEN H. HANSEN[2], LARS NIELSEN[3], AND KLAUS MOSEGAARD[4]

Geological Society of Denmark
https://2dgf.dk

Received 31 January 2022
Accepted in revised form
20 June 2022
Published online
15 August 2022

Lorentzen, M. C. L., Bredesen, K., Smit, F. W. H., Hansen, T. H., Nielsen, L. and Mosegaard, K. 2022: Mapping Cretaceous faults using a convolutional neural network – A field example from the Danish North Sea. Bulletin of the Geological Society of Denmark, Vol. 71, pp. 31–50. ISSN 2245-7070.
https://doi.org/10.37570/bgsd-2022-71-03

The mapping of faults provides essential information on many aspects of seismic exploration, characterisation of reservoirs for compartmentalisation and cap-rock integrity. However, manual interpretation of faults from seismic data is time-consuming and challenging due to limited resolution and seismic noise. In this study, we apply a convolutional neural network trained on synthetic seismic data with planar fault shapes to improve fault mapping in the Lower and Upper Cretaceous sections of the Valdemar Field in the Danish North Sea. Our objective is to evaluate the performance of the neural network model on post-stack seismic data from the Valdemar Field. Comparison with variance and ant-tracking attributes and a manual fault interpretation shows that the neural network predicts faults with more details that may improve the overall geological and tectonic understanding of the study area and add information on potential compartmentalisation that was previously overlooked. However, the neural network is sensitive to seismic noise, which can distort the fault predictions. Therefore, the proposed model should be treated as an additional fault interpretation tool. Nonetheless, the method represents a state-of-the-art fault mapping tool that can be useful for hydrocarbon exploration and CO_2 storage site evaluations.

Keywords: Machine learning, fault detection, cap-rock integrity, reservoir modelling, Cretaceous, Danish North Sea.

[1]*Department of Geophysics and Sedimentary Basins, Geological Survey of Denmark and Greenland (GEUS), Øster Voldgade 10, 1350 Copenhagen, Denmark.* [2]*Department of Geoscience, Aarhus University, Høegh-Guldbergs Gade 2, Aarhus C, Denmark.* [3]*Department of Geosciences and Natural Resource Management, University of Copenhagen, Øster Voldgade 10, 1350 Copenhagen, Denmark.* [4]*Niels Bohr Institute, University of Copenhagen, Blegdamsvej 17, 2100 Copenhagen, Denmark.* [*]*Correspondence: mlo@geus.dk.*

Fault mapping is a crucial seismic interpretation task that provides valuable structural information for prospect evaluation, seal integrity studies, and drilling operations targeting reservoirs in hydrocarbon and green energy applications. As faults may act as potential migration pathways of pore-fluids or baffles to fluid flow, it is important to outline their spatial network, density, and connectivity (Sorkhabi & Tsuji 2005; Fossen 2016; Smit *et al*. 2018). Furthermore, fault mapping and visualisation in 2D section and map view provide insights into the tectonic evolution of an area. If vertical displacements are larger than the seismic resolution, faults may appear as discontinuities in the layered reflectivity, and their presence may scatter the energy and distort the seismic imaging. Manual interpretation of faults can be a tedious and time-consuming process, and their location and extent are not always clearly apparent in seismic data. To highlight these discontinuities, a standard procedure is to use some edge detection seismic attributes such as semblance (Marfurt *et al*. 1998), coherency (Marfurt *et al*. 1997), and variance (van Bemmel & Pepper 2000;

Randen *et al*. 2001). These attributes rely on lateral changes in seismic reflection (dis)continuity as well as alterations in the frequency content (Chopra & Marfurt 2007). However, a pitfall of these methods for fault interpretation is that these attributes also highlight lithological or stratigraphical facies variations and seismic noise.

In recent years, machine learning methods have successfully been implemented in the geoscience domain for a wide range of applications, such as horizon tracking, salt dome identification, facies classification and fault mapping (Dramsch 2020). The fault mapping challenge can generally be regarded as a basic image segmentation task by pixel-wise classifying the input seismic data as either background (seismic data) or fault location. The pixel dimensions correspond to the dimensions of the acquisition setup in terms of inline and crossline spacing and sample interval.

In a supervised learning framework, a convolutional neural network (CNN) approach can be used to identify the location of faults in seismic data based on a synthetic training set or manual or automated fault picks in seismic data. Therefore, this CNN approach does not require the calculation of seismic attributes to identify the location of potential fault zones (Wu *et al*. 2019; Wrona *et al*. 2020). Previous studies have successfully implemented and demonstrated applications of neural networks for fault mapping and delineation. A supervised learning system to map simple fault networks in the subsurface using raw seismic recordings was proposed by Araya-Polo *et al*. (2017). Their neural network model was trained and tested on 3D synthetic seismic data and they concluded that more complex fault structures were required in the synthetic data to enhance the mapping quality. It was demonstrated by Wrona *et al*. (2020) how cropped 2D samples with manually labelled faults from large 2D seismic sections from the northern North Sea could be used in a supervised learning framework for identifying faults in 2D sections. They compared two different CNN models: (1) a simple 2D CNN model that downsamples the cropped input image and classifies it, and (2) a 2D U-Net model (based on the work of Long *et al*. 2015; Ronneberger *et al*. 2015) that labels the cropped input image pixel-wise. Both approaches had similar fault mapping accuracy in the seismic section but differed significantly in computation time for these test predictions (2 hours for the simple CNN versus 5 seconds for the U-Net).

It was demonstrated by Wu *et al*. (2019) with limited computational resources, how a simplified version of the U-Net structure could accurately predict faults

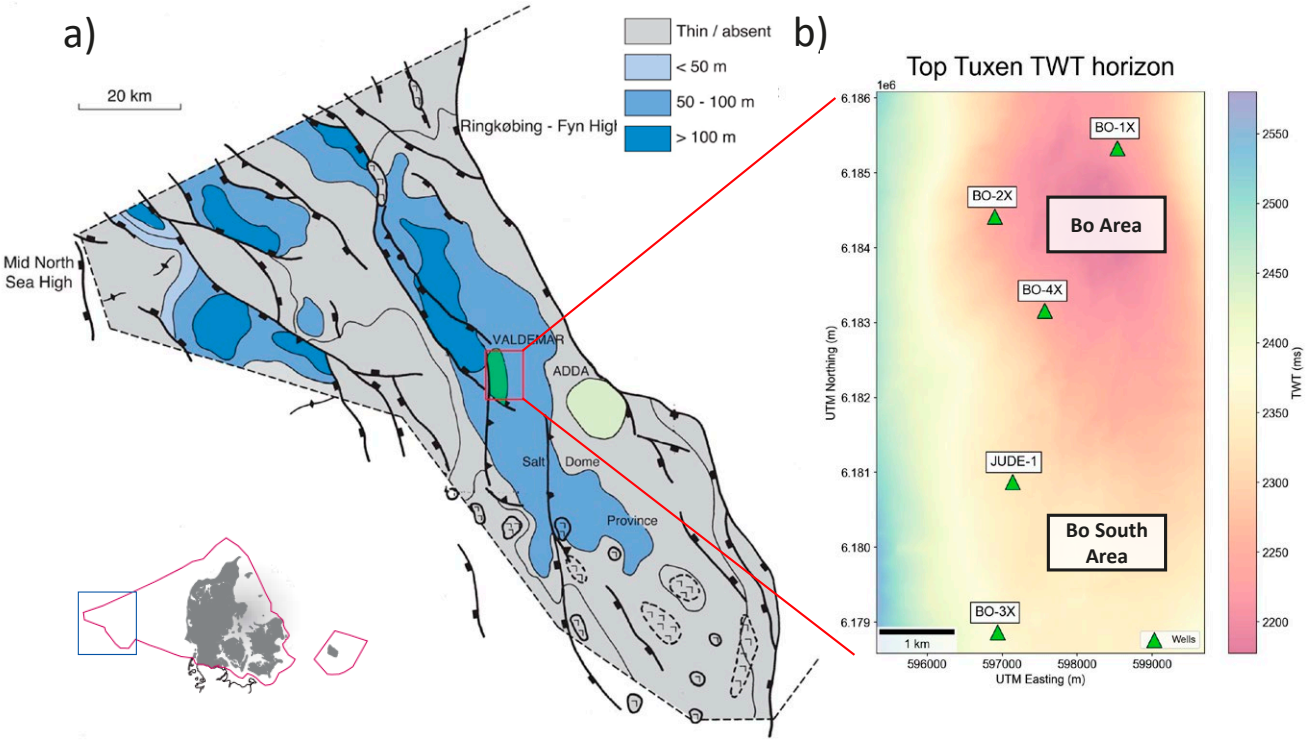

Fig. 1: a) Location of the Danish Central Graben and thickness map of the Sola and Tuxen formation. The Valdemar Field with the various Bo wells is outlined in the red rectangle (modified figure from Jakobsen *et al*. 2004). **b)** Map of the Bo and Bo South areas (part of the larger structure, Bo-Jens Ridge) in the Valdemar Field with Top Tuxen two-way traveltime (TWT) structure and relevant well locations.

in 3D seismic data by training on synthetic data. In their study, the trained U-Net CNN outlines realistic fault interpretations in various 3D seismic surveys including the Netherlands F3 Block and a subduction zone at the Costa Rica margin. Following that work a fault detection machine learning competition was held in 2020 by the Norwegian Petroleum Directorate (Bormann *et al*. 2020). The competition used synthetic seismic data and non-optimal real seismic data from the Itchys Field located on the NW Shelf of Australia for training and testing different supervised learning models. The fault mapping results were rated by human interpreters to assess the quality of the mapping, and none of the competitors was given a significantly high score. It was suspected that the low success rate was related to migration artifacts remained in the seismic data due to sub-optimal processing that was used for the test phase.

Other studies have modified the CNN structure proposed by Wu *et al*. (2019) and used it as a state-of-the-art benchmark model for automatic fault interpretations trained on either synthetic data, real data with interpretations or a combination of the two. A suite of models including the U-Net CNN was used in a study by An *et al*. (2021). By applying the models on two real test data sets, Inner Moray Firth (UK North Sea sector) and Thebe Gas Field (NW Shelf of Australia), they demonstrated that the test predictions of the U-Net CNN could be improved by implementing image augmentation methods and manually labelled field data in the training data. In a study by Dou *et al*. (2021), they show how a combination of 3D synthetic data and 2D labelled real data from the Shengli Oilfield in China could be used in the training process to improve the U-Net CNN model performance and ability to generalise to other seismic surveys.

In all the former cases, the U-Net CNN model seems in agreement with traditional fault-enhancing attributes and other proposed machine learning models, which indicates a good generalisation ability across seismic surveys of varying quality and with different faulting systems (Wu *et al*. 2019; An *et al*. 2021; Dou *et al*. 2021).

In this study, we apply the open-source U-Net CNN (hereafter referred to as 'CNN') model by Wu *et al*. (2019) that has been trained on synthetic seismic data generated by a convolutional model with planar-shaped faults on post-stack data from the Valdemar Field located in the Danish North Sea (Fig. 1a). We focus on Cretaceous succession comprising an upper and lower part. Fig. 2 shows a stratigraphic column covering the Cretaceous section in the Danish Central Graben (DCG). Whereas the Upper Cretaceous (UC) is regionally composed of thicker high-porosity pure chalk reservoir intervals, the Lower Cretaceous (LC),

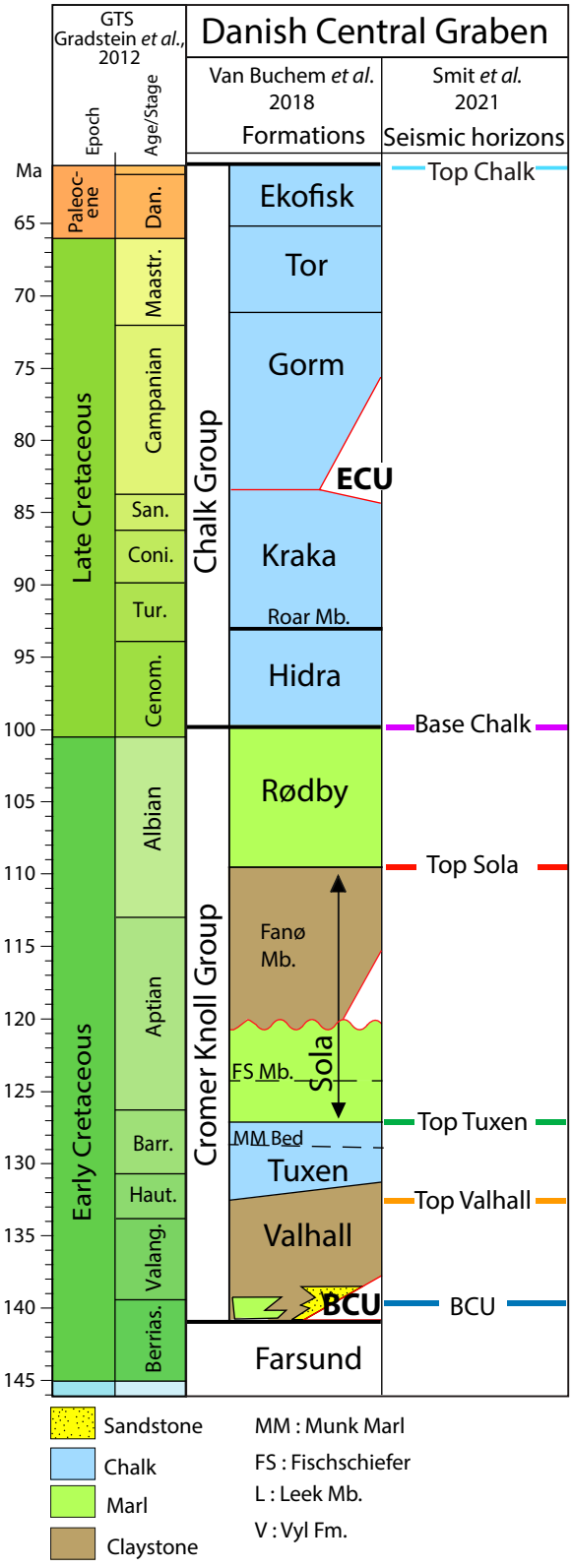

Fig. 2: Stratigraphic column scheme of the Cretaceous succession in the Danish Central Graben adapted from van Buchem *et al*. (2018). Coloring of the key seismic horizons used throughout the study from Smit *et al*. (2021) can be seen in the right section of the figure.

which also contains reservoir layers, is thinner and more heterogeneous with marly chalks and low matrix permeabilities (Jakobsen *et al*. 2004). The fine-grained shale can potentially be integrated in fault zones of the LC succession and work as barrier to fluid flow (Fossen 2016). Seismic interpretation and coherency studies of the Valdemar Field was conducted by Madsen & Britze (1999) as a part of the multi-institutional PRIORITY research programme (1997–2002) and they concluded that conventional fault mapping methods were insufficient to map the fault complexity of the field in the complete Cretaceous succession. More recently, Bredesen *et al*. (2021) performed a quantitative seismic interpretation study to outline reservoir quality variations and to boost the resolution of the LC succession in the Valdemar Field. Their study showed that the seismic image of the LC interval was characterised by limited resolution and by interfering multiple energy from the overlying UC chalk succession. This is caused by the chalk succession having a higher seismic velocity than the LC mudstones and chalks, which generates scattering, interfering multiples and converted waves (Vidalie *et al*. 2012; Montazeri *et al*. 2018).

The objective of this study is to evaluate the performance of the CNN model by Wu *et al*. (2019) on the Valdemar Field data and review the outlined faults by comparison to manually interpreted faults and a simple industrial standard workflow procedure with variance and intelligent ant-tracking (Pedersen *et al*. 2002). Firstly, we review the structural geology in a regional and local setting. Secondly, we outline how the CNN model and its training process work and address the data conditioning steps of the seismic data from the Valdemar Field. Finally, we analyse the results and discuss some of the shortcomings of the study as well as delineate potential improvements.

Geological background

Regional framework

The Valdemar Field is located in the central part of the DCG, occurring in the westernmost part of the Danish offshore sector (Fig. 1a). The DCG comprises a complex of fault-bounded basins and highs and is part of the system of failed rifts that spans the North Sea area (Ziegler 1990). During the Late Jurassic, tectonic extension generated a series of roughly NW–SE-trending half-graben bounded by large normal faults in the area (Møller & Rasmussen 2003). As a result of Late Jurassic rifting, subsidence of these basins caused the accumulation of thick successions of largely marine shale, including organic-rich units that are modern-day sources of hydrocarbons (Fig. 2) (Ineson 1993; Ineson *et al*. 2003). In the DCG, rifting ceased around the onset of the Early Cretaceous (Møller & Rasmussen 2003), but the rift-related basin morphology persisted throughout the Early Cretaceous along with the deposition of the Cromer Knoll Group deposits (Vejbæk 1986).

During the Late Cretaceous and Paleogene, regional tectonic shortening caused basin inversion and relative uplift of former rift depocentres (Vejbæk & Andersen 2002; van Buchem *et al.* 2018). This generated several structural traps with Cretaceous reservoirs in the area.

Local structural framework

The Valdemar Field contains hydrocarbon within the Cretaceous successions and occurs on the crest of a large anticlinal fold (the Bo–Jens Ridge), which formed during Late Cretaceous inversion and strikes approximately North–South (Vejbæk & Andersen 2002; Hansen *et al*. 2021). Locally within the field perimeter, a saddle point separates two gentle structural highs near the wells North Jens-1 and Bo-1X at reservoir levels (Jakobsen *et al*. 2005). This configuration arose due to varying degrees of reactivation of, and folding along, rift-related faults below the reservoir (Hansen *et al*. 2021). Groups of small normal faults (some with offsets near the limit of seismic resolution) populate the crest of Bo–Jens Ridge at Cretaceous levels. These faults are interpreted by Hansen *et al*. (2021) as the result of a combination of outer-arc extension and gravitational collapse during inversion and folding. Fig. 1b shows the southern downflank of the southern Bo–Jens Ridge with marked well locations. This outlines the area of interest for our study as it remains an immature part of the Valdemar Field.

Convolutional neural network

In this research, we use the previously trained version of the CNN model by Wu *et al*. (2019) to predict the faults in a 3D post-stack survey from the Valdemar Field based on the work of Bredesen *et al*. (2021). Two seismic processing steps are introduced for this study to make it suitable for the CNN fault prediction. Firstly, the post-stack data are filtered using an automatic gain control (AGC) to increase the weak signals of the LC. The amplitudes are increased to make the CNN fault labelling more accurate, however, the noise will be amplified as well, and there is a potential risk of the CNN predicting faults in the noisy areas. Secondly, after the AGC process the seismic data are normalised

by subtraction of its mean value and division by its standard deviation to make the amplitude ranges consistent with the synthetic training from Wu *et al.* (2019).

The visual effects of the two-step conditioning on the seismic data are shown at Fig. 3. The AGC-filtered seismic will be used for all the following figures to

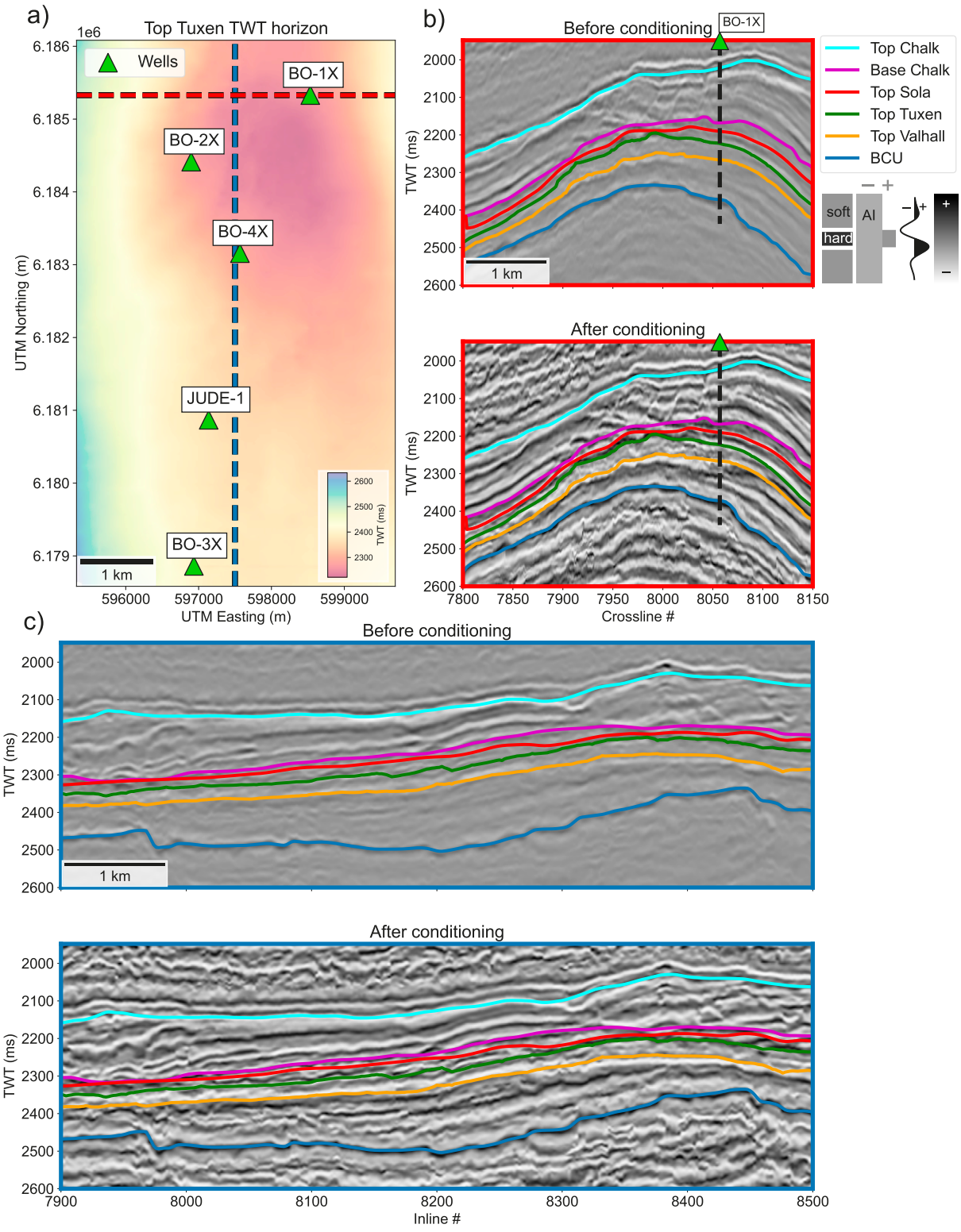

Fig. 3: a) Map of the Tuxen horizon in two-way traveltime (TWT) in the Valdemar Field with well locations. The dashed red and blue lines indicate the crossline and inline sections shown in **b)** and **c)**, respectively.

improve the visualisation of the LC succession. Note that inline and crossline sections shown throughout the study will be influenced by a vertical exaggeration. The European polarity convention shown in Fig. 3 will be used for all seismic data displayed in the study. The main horizons of the LC used in this study originate from the regional interpretation study by Smit *et al*. (2021).

A detailed description of the mathematics and architecture of the CNN model and its U-Net structure is beyond the scope of this study, and the reader is referred to the papers by Ronneberger *et al*. (2015) and Long *et al*. (2015). The main framework of the U-Net applied in this study is composed of two phases. Firstly, the 3D seismic volume is spatially reduced in steps to create a so-called feature vector. The feature vector contains filtered information from the seismic cubes through a series of matrix operations. Secondly, the downsampling process is followed by an upscaling operation, and the final feature layer holds extracted information from the seismic cube in terms of a fault cube of the same size as the original 3D seismic input.

The CNN model is trained using 200 synthetic seismic and fault cubes of dimensions (128×128×128) elements resembling seismic volumes of (1.6km×3.2km×512ms) by 12.5 meters inline and crossline spacing (considering every second crossline) and 4ms sample interval. The workflow for generating the synthetic data originates from Wu & Hale (2016). Here, they use a series of reflections between -1 and 1 includes folding structures and planar shearing to mimic true geological variations. Sequentially, planar faulting is generated in the cubes with dips ranging from 65°-85°, and the perturbed reflection cubes are convolved with a Ricker wavelet with pre-defined varying frequency content. Lastly, Gaussian noise is added to the synthetic cube yielding various signal-to-noise ratios. Compared to real seismic data, the synthetic data are convenient to use for CNN model training as they allow better control on the ground truth fault labels and thus avoid marking errors based on misinterpretations. The ground truth fault labels are located in binary cubes (zeros indicate non-fault, and ones indicate faults) of the same dimensions as the seismic cube. Moreover, using synthetic data render possible a great quantity of training data that can be difficult to obtain from real seismic data. To assess the similarity between the synthetic training data and the Valdemar Field data, Fig. 4a and 4b shows a training data slice and a cropped section of the

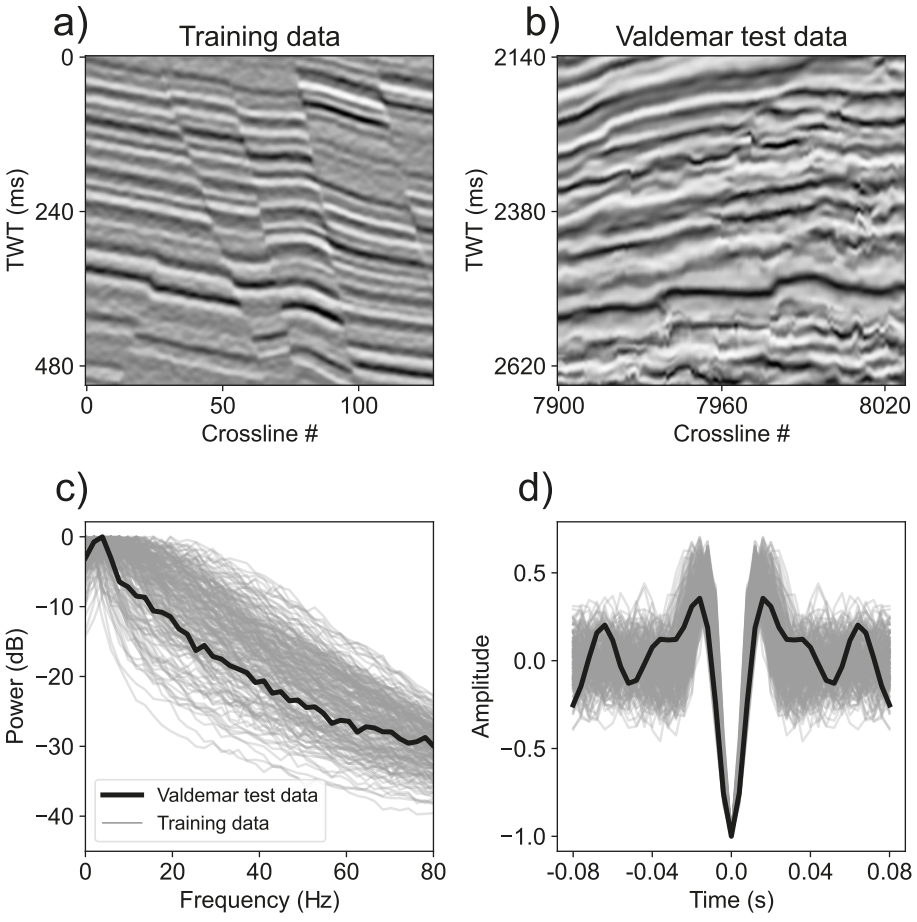

Fig. 4: Samples of crossline sections of **a)** synthetic training data and **b)** Valdemar Field data from the Cretaceous section (test data). The frequency spectrum of all 200 3D training cubes and the Valdemar test data is shown in **c)**, and their wavelets are shown in **d)**.

conditioned Valdemar test data from the Cretaceous section, respectively. Some visual discrepancies are observed between the training and test sample as the Valdemar data seems more blurred and distorted than the synthetic sample. This could be caused by noise left in the seismic volume after processing from e.g. interfering multiples. Nonetheless, Fig. 4c and 4d show the frequencies and wavelets of all training data 3D cubes versus the Valdemar Field Cretaceous test data, respectively, and indicate that the frequencies and wavelet form of the latter are well-represented in the training data.

The CNN training involves passing all the synthetic seismic cubes through the U-Net structure, estimating the error between the predicted fault labels and the ground truth faults, and adjusting the weights of the CNN accordingly. Hence, the training process can be regarded as an optimisation process that aims to minimise the difference between the predicted fault label and the ground truth fault label. The end result is a cube with an assigned CNN fault probability for each pixel. Fig. 5 shows a series of slices from the

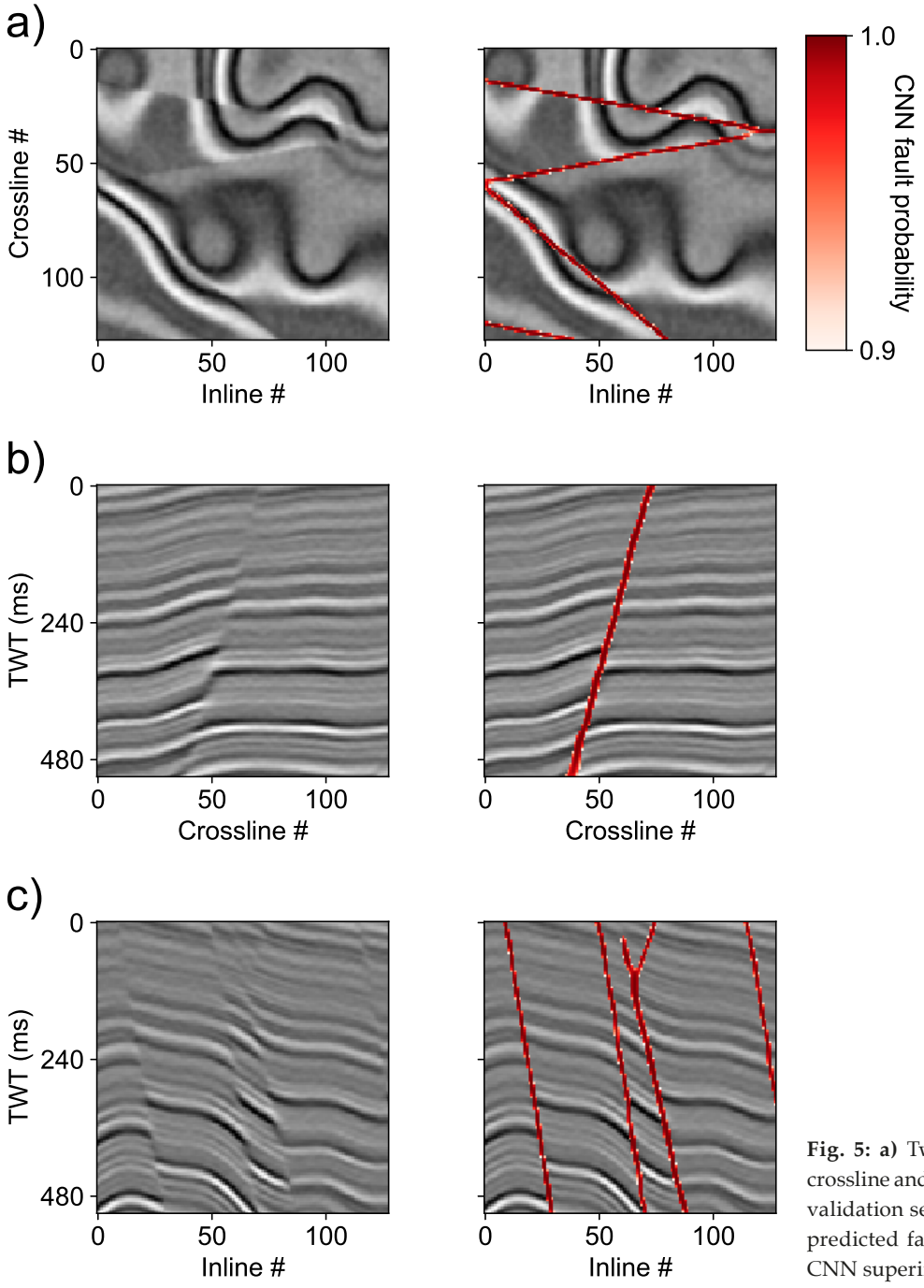

Fig. 5: a) Two-way traveltime (TWT), **b)** crossline and **c)** inline sections of a synthetic validation seismic cube in left column and predicted fault probability by the trained CNN superimposed in right column.

synthetic validation cube, which was not a part of the training process, with the fault predictions from the trained CNN model. We chose to show the > 90% of CNN fault probability throughout the study with the intention of ensuring a high level of confidence in the potential faults displayed. It should be stated that the CNN fault probability does not reflect true fault probability, but indicates the CNN model's posterior likelihood of a fault being present in a given dataset based on the learning and extracted features from the synthetic training data. Based on the synthetic samples used for training, the CNN model is applied to the conditioned seismic data from the Valdemar Field.

Variance and ant-tracking

The variance seismic attribute is a measure of spatial discontinuity. It is known as an edge detection process as it represents the lateral variability in a defined sample interval. The size of the sample interval determines the detail of fault features to be resolved, and the method is sensitive to both waveform and lateral changes of the reflection amplitude (Chopra & Marfurt 2007). For the interpreter, time slices of a variance volume or a similar edge attribute can be a great help when manually picking faults from vertical seismic sections. This makes it easier to stick to the same fault trace while scrolling through the data several inlines or crosslines at a time. Moreover, a so-called ant-tracking filter (Pedersen *et al*. 2002) can be applied to the variance attribute that further enhances surface-like features by a pre-defined set of orientation ranges and step sizes. This allows extracting features that resemble those of faults based on the variance while limiting the amount of random noise in the attribute. Both the variance attribute and ant-tracking filter will be used to compare with the CNN model predictions.

The post-stack seismic volume prior to the AGC-filtering as represented in upper plots of Fig. 3b and 3c is used as input for the variance attribute computation as the seismic attribute calculation does not require any pre-conditioning. From the variance attribute, the ant-tracking filter is applied. The details of the parameters for the variance and ant-tracking features are listed in Table 1.

Table 1. Input parameters of the variance and ant-tracking features. The Petrel E&P Software is used for the computations of the attributes.

Variance input parameters	
IL range	3
XL range	3
Vertical smoothing	15 samples (60 ms)
Window range	1 sample (4 ms)
Dip correction	off
Ant-tracking input parameters	
Ant mode	Passive
Initial ant boundary	7
Ant-track deviation	2
Ant step size	3
Illegal steps allowed	1
Legal steps required	3
Stop criteria (%)	5

Manual interpretations

A manual fault interpretation on the corresponding area from a regional 3D seismic volume (for details on this dataset, see Hansen *et al*. 2021) will be used to show what an interpreter with structural geological expertise would map in the area. It should be noted that the interpretation was performed on a depth-converted seismic volume that intersects with the Valdemar Field using both inlines, crosslines and variance maps of the Top Chalk, Base Chalk and Base Cretaceous Unconformity (BCU) horizons (Fig. 2). The fault offsets in the study area are relatively small compared to the vertical seismic resolution, which is around 30 meters for the section (Bredesen *et al*. 2021), and many show offsets that are near the limit of robust manual interpretation. It should be stated clearly that we do not consider the manual interpretation as a ground truth, but as an additional binary fault prediction attribute based on standard seismic attributes. The seismic attribute calculations and interpretations were achieved using another commercial software (Paleoscan) than what was used for the variance and ant-tracking features in this study. However, no major discrepancies are suspected, and the provided variance attribute as listed in Table 1 should be satisfying for the comparison purpose. In order to analyse the results, the depth of picked faults has been converted to two-way traveltime via the same velocity model that was used for generating the depth-converted volume.

CNN model results and comparison

A suite of the key Cretaceous horizons with superimposed CNN fault predictions can be seen in the following Figures: Top Chalk in Fig. 6, Base Chalk in Fig. 7, Sola horizon in Fig. 8, Tuxen horizon in Fig. 9, Valhall horizon in Fig. 10, and BCU horizon in Fig. 11.

Note that the seismic sections in the plots have slightly been brightened to contrast the superimposed

features. Both the manual interpretation and the CNN model are accompanied by a strike fault diagram to show the overall fault trends for the shown maps. According to the fault strike diagrams of both the manual interpretation and the CNN models, a general NE–SW-trend is dominating throughout the

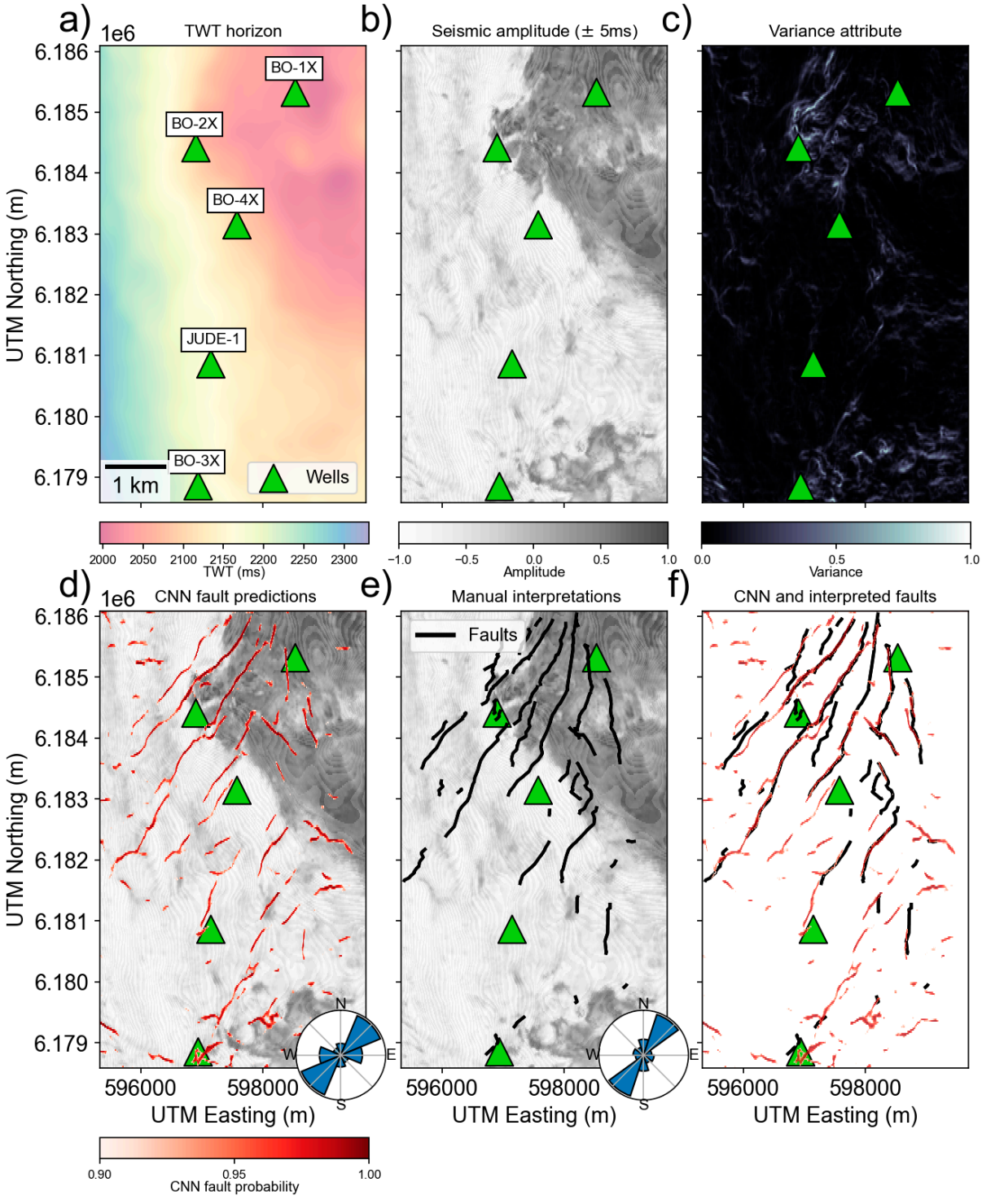

Fig. 6: a) Map of the Top Chalk horizon in two-way traveltime (ms). **b)** Averaged seismic amplitudes in a ± 5 ms window around the horizon. **c)** Variance attribute extracted along the horizon. **d)** CNN fault predictions (red colouring) and **e)** manual fault interpretations (black lines) along the horizon superimposed on the ± 5 ms seismic window with fault strike diagrams. **f)** CNN fault predictions superimposed with manual fault interpretations.

Cretaceous section in the Valdemar Field. The faults picked by the CNN model pose detailed and realistic interpretations when viewed on horizon maps. They are generally in agreement with the variance maps along the same horizons, in which relatively clear fault patterns are evident (e.g. Fig. 7 and Fig. 11).

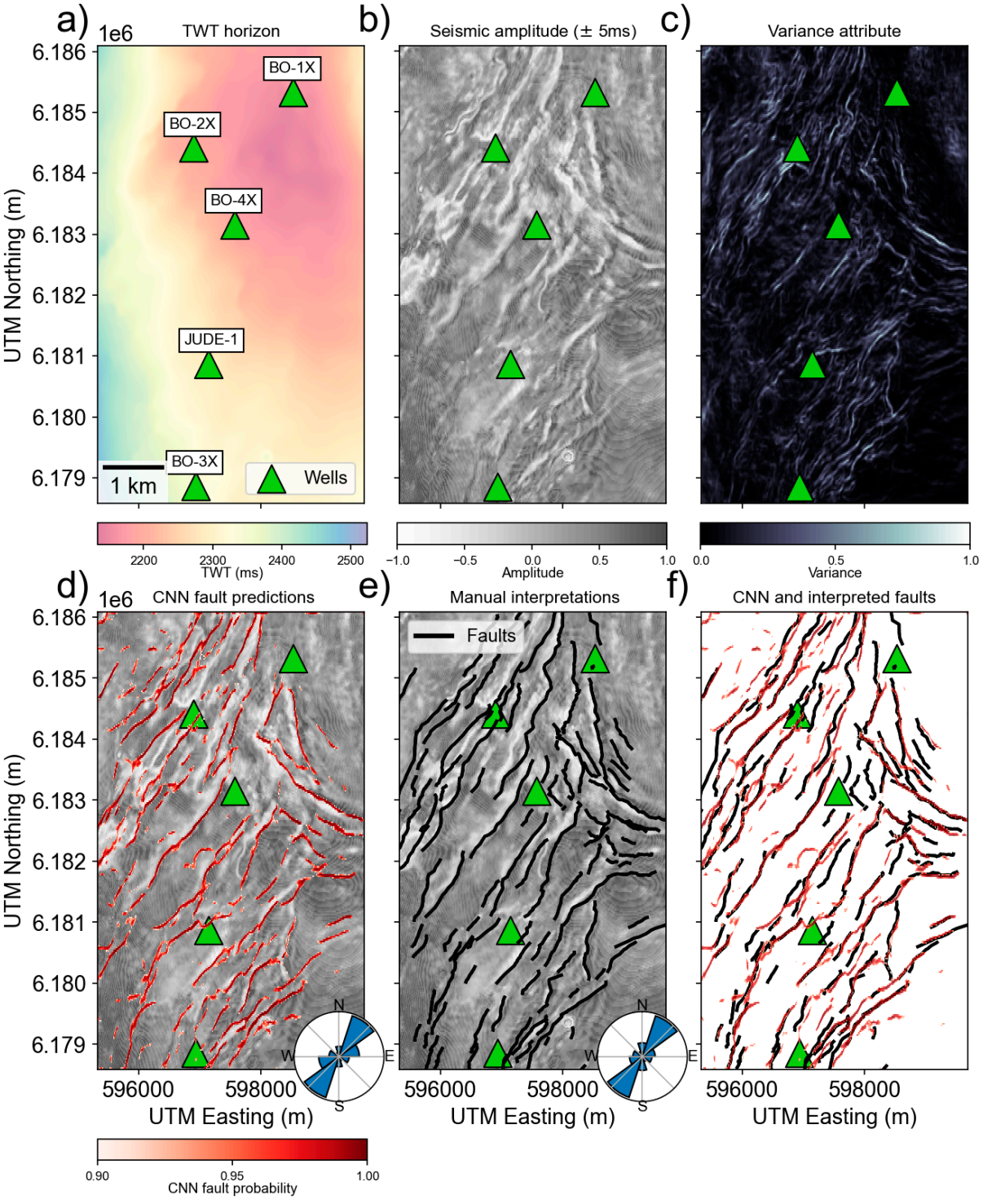

Fig. 7: a) Map of the Base Chalk horizon in two-way traveltime (ms). **b)** Averaged seismic amplitudes in a ± 5 ms window around the horizon. **c)** Variance attribute extracted along the horizon. **d)** CNN fault predictions (red colouring) and **e)** manual fault interpretations (black lines) along the horizon superimposed on the ± 5 ms seismic window with fault strike diagrams. **f)** CNN fault predictions superimposed with manual fault interpretations.

They also coincide well with the manually interpreted faults when viewed in this manner. A limited amount of manually interpreted faults are observed for the Top Tuxen and Top Valhall horzons (Fig. 9 and Fig. 10). It is suspected that this is related to interpretation was carried out using only the Top Chalk, Base Chalk and

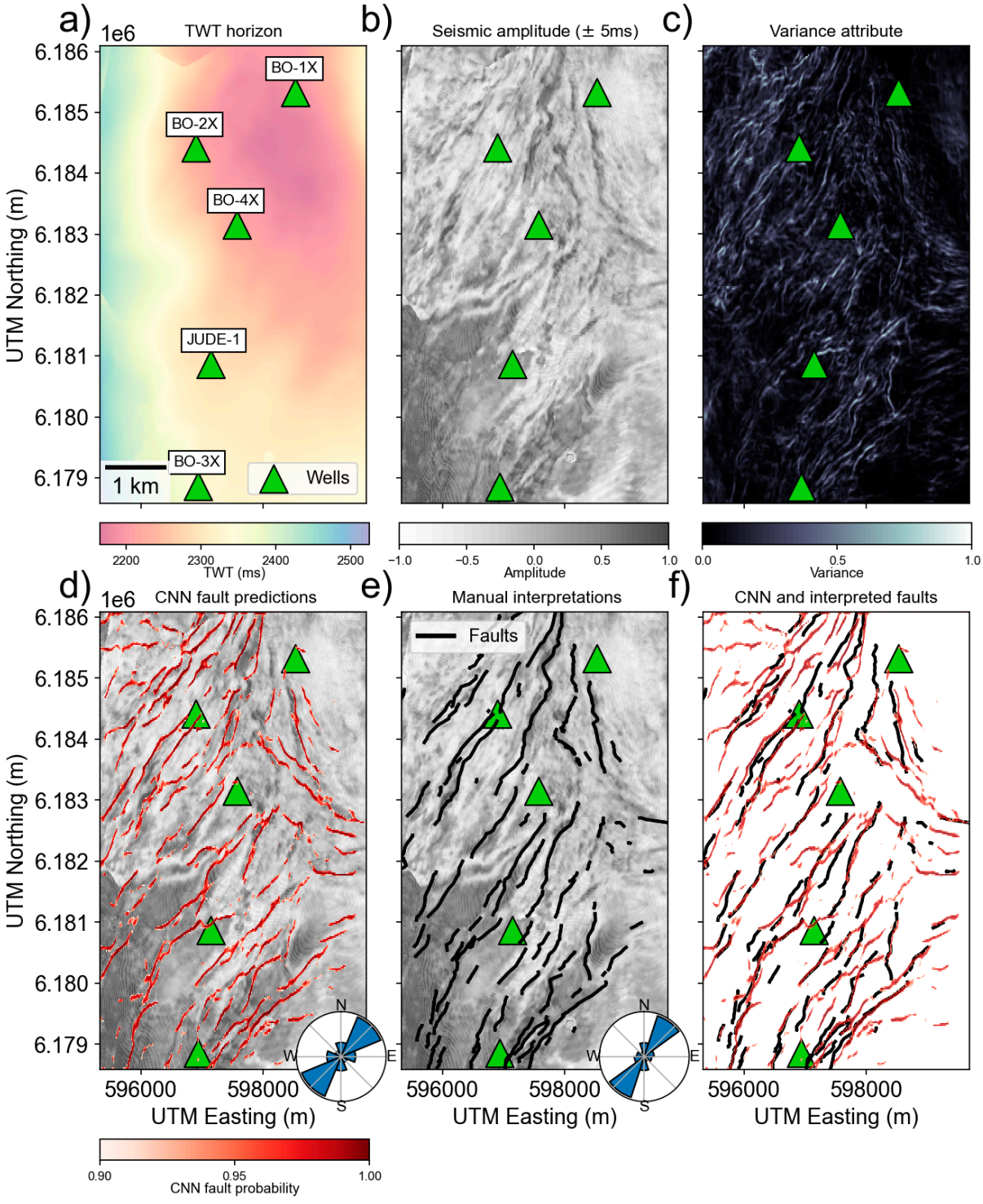

Fig. 8: a) Map of the Sola horizon in two-way traveltime (ms). **b)** Averaged seismic amplitudes in a ± 5 ms window around the horizon. **c)** Variance attribute extracted along the horizon. **d)** CNN fault predictions (red colouring) and **e)** manual fault interpretations (black lines) along the horizon superimposed on the ± 5 ms seismic window with fault strike diagrams. **f)** CNN fault predictions superimposed with manual fault interpretations.

BCU horizons, and therefore lacking details around the Tuxen and Valhall section of the survey. The CNN model provides a level of detail in the picked faults that surpasses that of the manual interpreter who only picks the faults from a fraction of the vertical seismic sections. Specifically, the close overlaps of individual

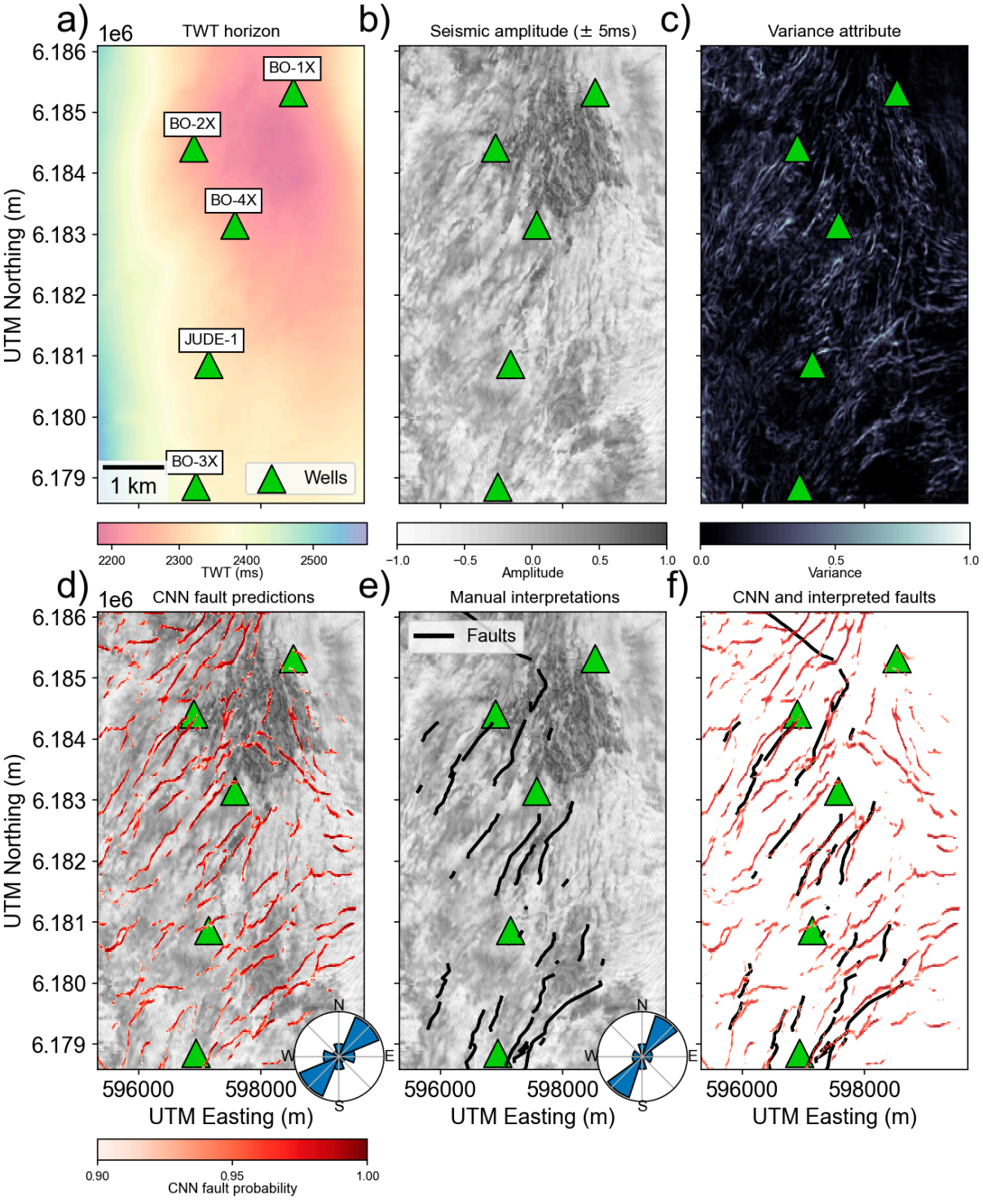

Fig. 9: a) Map of the Tuxen horizon in two-way traveltime (ms). **b)** Averaged seismic amplitudes in a ± 5 ms window around the horizon. **c)** Variance attribute extracted along the horizon. **d)** CNN fault predictions (red colouring) and **e)** manual fault interpretations (black lines) along the horizon superimposed on the ± 5 ms seismic window with fault strike diagrams. **f)** CNN fault predictions superimposed with manual fault interpretations.

faults and jogs in fault traces (caused by the merging of smaller fault segments during growth) are picked out nicely with good lateral consistency, whereas the manual interpreter would mostly pick only single linear fault segments across them. An example of this can be seen in (marked with blue circle in Fig. 11f)

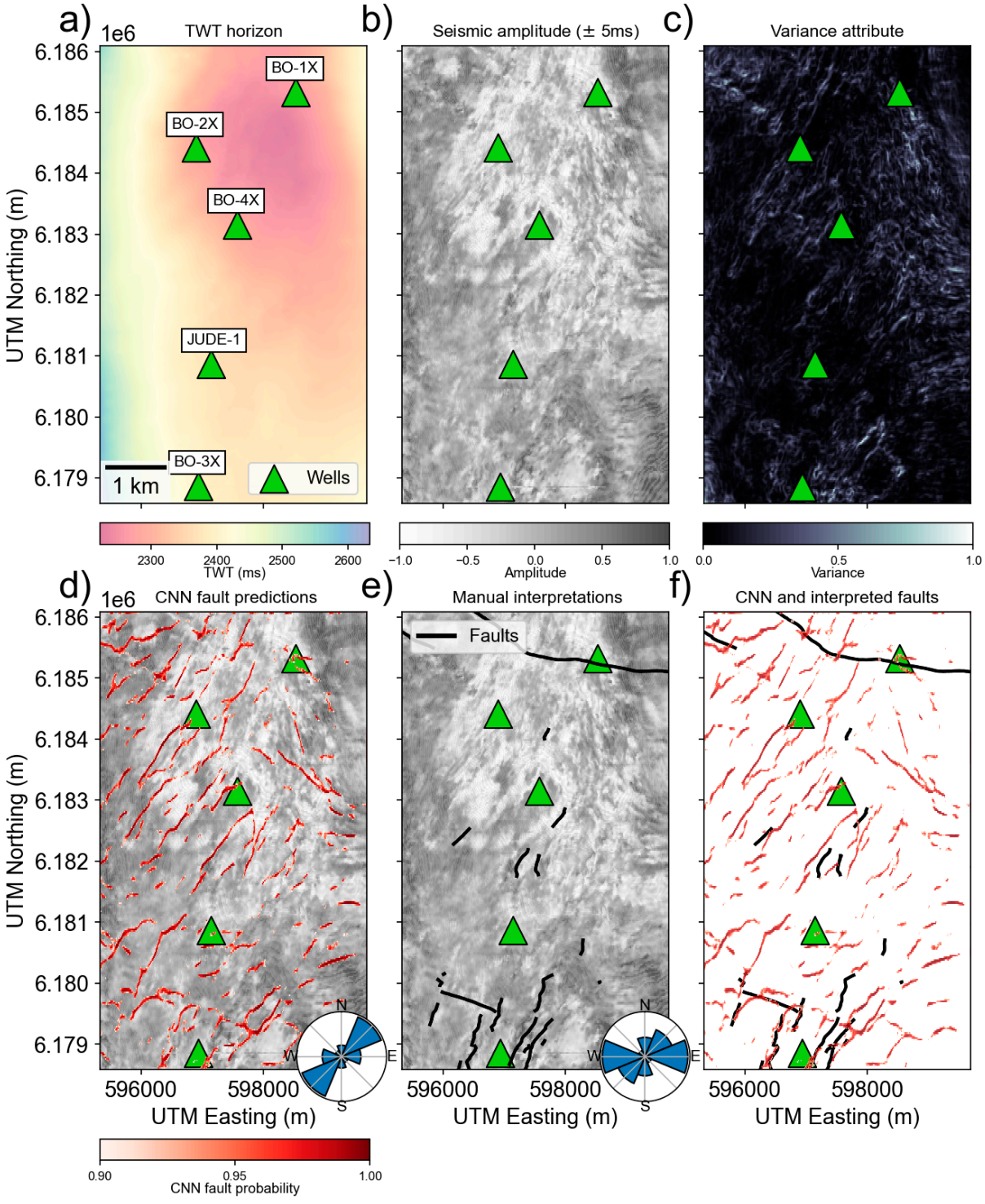

Fig. 10: a) Map of the Valhall horizon in two-way traveltime (ms). **b)** Averaged seismic amplitudes in a ± 5 ms window around the horizon. **c)** Variance attribute extracted along the horizon. **d)** CNN fault predictions (red colouring) and **e)** manual fault interpretations (black lines) along the horizon superimposed on the ± 5 ms seismic window with fault strike diagrams. **f)** CNN fault predictions superimposed with manual fault interpretations.

just below well Bo-4X. Here, the jogs where two faults have connected during lateral growth is mapped in detail by the CNN model, whereas neither the variance attribute nor the manual interpreter picks up

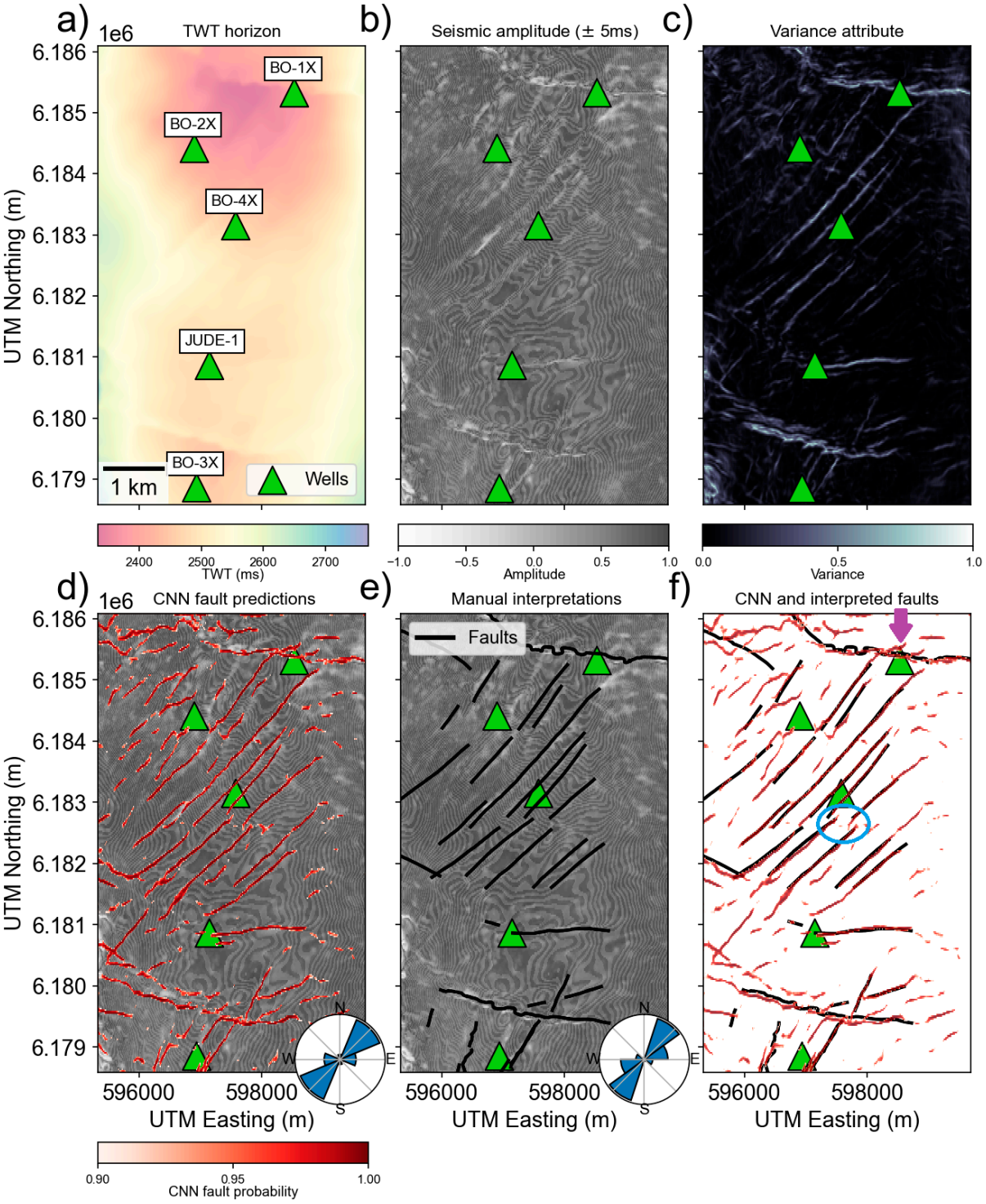

Fig. 11: a) Map of the Base Cretaceous Unconformity (BCU) horizon in two-way traveltime (ms). **b)** Averaged seismic amplitudes in a ± 5 ms window around the horizon. **c)** Variance attribute extracted along the horizon. **d)** CNN fault predictions (red colouring) and **e)** manual fault interpretations (black lines) along the horizon superimposed on the ± 5 ms seismic window with fault strike diagrams. **f)** CNN fault predictions superimposed with manual fault interpretations. The blue circle in f) highlights two jogs where faults have connected during lateral growth that are not represented in the variance attribute nor the manual interpretation.

this feature. Displayed upon stratigraphy-consistent horizons, the faults predicted by CNN appear realistic and overall in accordance with the manual interpretation and the seismic variance attribute.

Figures 12 and 13 show the crossline and inline sections displayed in Fig. 3 with superimposed results. The fault plots are accompanied by a dip attribute. It should be noted that the dip plots do not reflect the true angles due to the vertical exaggeration in the vertical sections. For simple planar fault segments in especially the Chalk Group (Fig. 2), the manual interpretation and the CNN model results seem to be in good agreement (green circles in Fig. 12c and Fig. 13c). However, some discrepancies are apparent between the dip angles of the CNN predictions and manual interpretations. In most cases, the CNN model predicts faults with larger dips than those of the manually interpreted faults, and less consistent, i.e. the CNN modelled faults often appear sinuous in the vertical sections (black circles in Fig. 12c and Fig. 13c). The most apparent detail in the CNN fault predictions and ant-tracking attribute of the crossline section (Fig. 12f) is in the lower-right region around the BCU horizon (marked with red circle). Here, the CNN predicts large areas to have a high probability of being faulted, and the same areas have high variance values (red circle in Fig. 13d). Considering the location of the crossline section (Fig. 3a, red dashed line), a WNW-ESE striking fault that runs sub-parallel to and intersects with the seismic section around Bo-1X has been outlined both manually and by CNN prediction at the BCU level (marked with purple arrow in Fig. 11f). Therefore, the faulting anomaly at BCU appears more as a plane rather than a line segment in the vertical section.

The ant-tracking filter agrees with the CNN model predictions in most cases as shown in Fig. 12f and Fig. 13f suggesting that the two methods track the same features in the seismic signals. Nonetheless, in the fault interpretation task of the Valdemar Field, the applied variance and ant-tracking filter can be problematic due to the ambiguity in the orientations of the fault features as well as outlining the extents of individual faults. A default set of input parameters was chosen for the variance and ant-tracking (Table 1), which shows the need to generate several iterations of variance and ant-tracking combinations in a trial and error fashion ideally limiting noise artefacts while preserving fault features. The CNN model does not require similar manual tuning as it is a part of the training process.

Discussion

The pre-trained CNN model from Wu *et al*. (2019) was used without any modifications of the model prior to applying it to the seismic data. It is important to have a healthy portion of scepticism about the training data that is put into the CNN model before making predictions in seismic data. This is due to the fact that the CNN model was trained on synthetic data, which raises a concern of to what extent the synthetic faults and seismic data represent the structural geology and seismic signals in the investigated area. It was suspected that the distortions observed in the Cretaceous succession of the Valdemar data originates from a combination of low signal-to-noise ratio and poor continuity of reflection events (Bredesen *et al*. 2021). Tailoring the synthetic data to resemble the seismic data from the Valdemar Field by e.g. using a statistical or deterministic wavelet from the seismic data instead of a Ricker wavelet and modifying the signal-to-noise ratio by adding or removing Gaussian noise could alter the fault predictions of the CNN model. It was seen in Fig. 4 that the wavelet and frequencies of the Valdemar data was well-represented in the training data. However, the cropped sections in Fig. 4a and 4b showed some visual dissimilarities with as the Valdemar data was more blurred and with poor reflection continuity. Data augmentation could be applied to make the training data more similar to the test data by implementing e.g. kernel filtering, resizing and rescaling and elastic (grid) deformation as a part of the training process. In the study by An *et al*. (2021), they conclude that vertical flip, emboss and elastic deformation substantially improves performance of the proposed machine learning models. The effect of the augmentation could be investigated by applying the CNN on the augmented data and, when trained, testing the new model on the Valdemar data and compare with the predictions presented in this research.

The pre-trained CNN has previously been applied on various seismic dataset representing different faulting systems with realistic fault predictions in agreement with other fault-enhancing seismic attributes and machine learning models, which indicates a good generalisation (Wu *et al*. 2019; An *et al*. 2021; Dou *et al*. 2021). However, it is questionable to what extent the trained CNN model is able to predict thrust and listric faults with low angle dips since these were not part of the training dataset. Low-angle faults were represented in the manual interpretation (Fig. 12a and 13a) whereas the CNN predicted faults were steeper (blue circles in Fig. 12c and 13c). The planar faulting in the synthetic data originating from Wu & Hale (2016) have dips ranging from 65°-85° corresponding to the seismic validation cube in Fig. 5. The high dip of the faults in

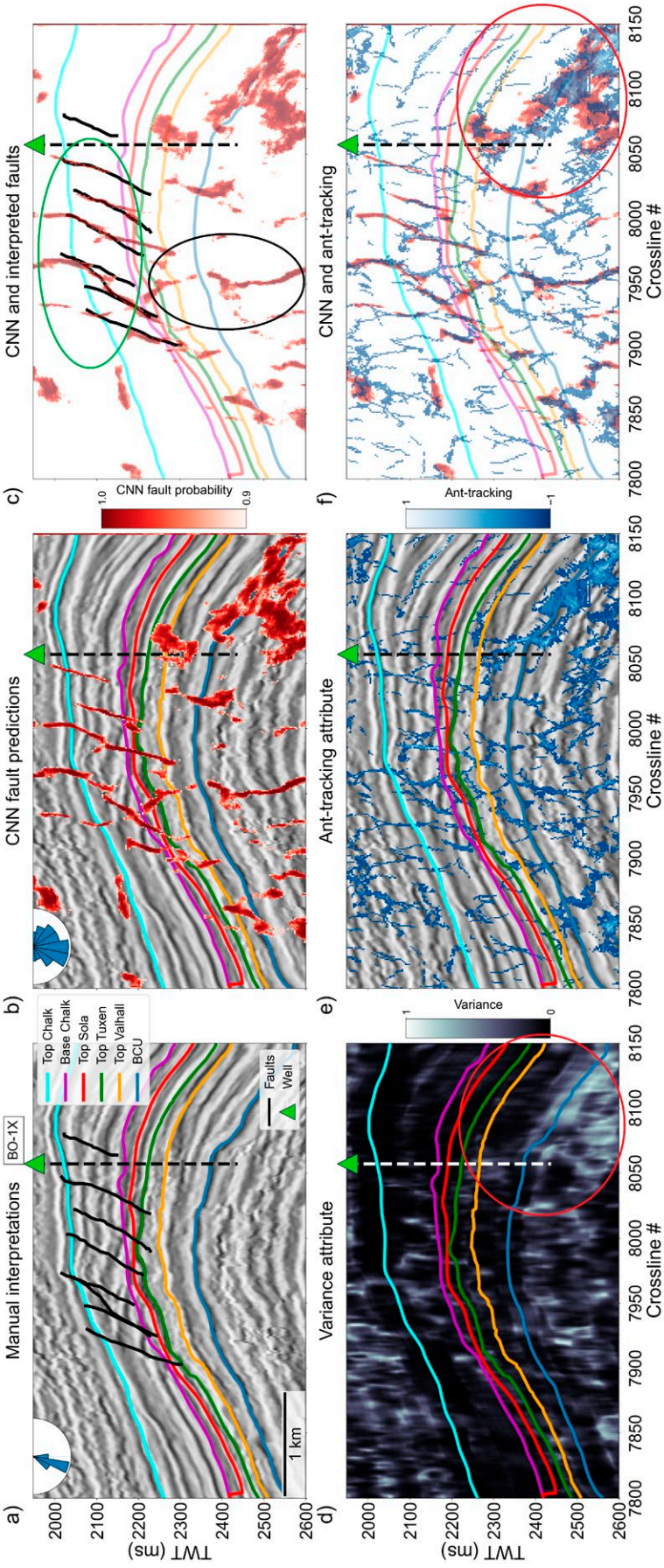

Fig. 12: Crossline section shown in Fig. 3a (dashed red) with **a)** intersecting manual interpretations and **b)** intersecting CNN predictions superimposed on the seismic section with dip attributes. **c)** CNN fault predictions superimposed with manual fault interpretations. The green circle highlights a good agreement between the two, and the black circle marks a discrepancy. **d)** Variance attribute and **e)** ant-tracking attribute extracted along the section superimposed on the seismic data. **f)** CNN fault predictions superimposed with ant-tracking attribute. The red circle indicates a parallel fault intersecting with the crossline section.

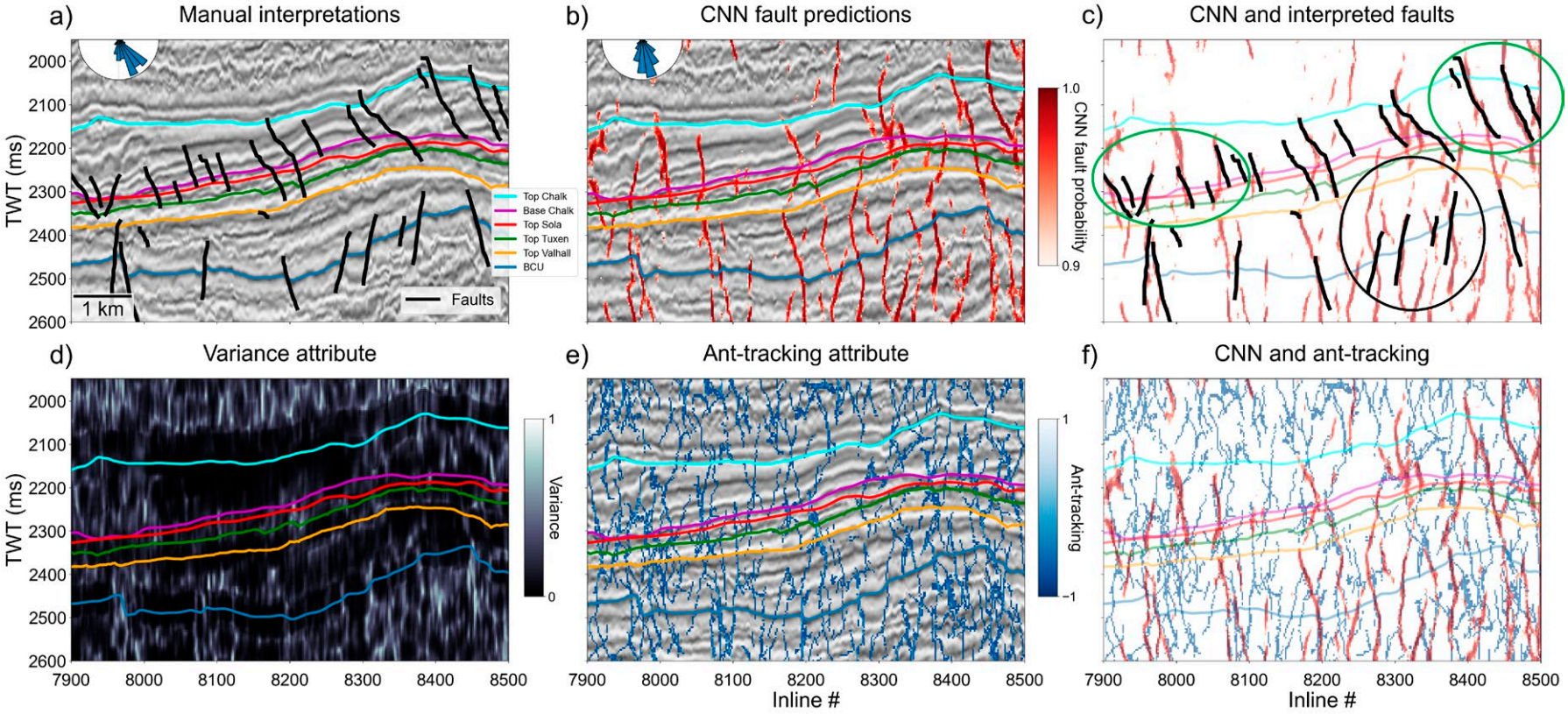

Fig. 13: Inline section shown in Fig. 3a (dashed blue) with **a)** intersecting manual interpretations and **b)** intersecting CNN predictions superimposed on the seismic section with dip attributes. **c)** CNN fault predictions superimposed with manual fault interpretations. The green circles highlight a good agreement between the two, and the black circle marks a discrepancy e) Variance attribute and **d)** ant-tracking attribute extracted along the section superimposed on the seismic data. **f)** CNN fault predictions superimposed with ant-tracking attribute.

the training data suggests that the CNN model has a bias towards predicting steeper faults limiting its ability to detect certain low-angle faults like thrust faults (Fossen 2016). One approach to test the hypothesis would be to apply the CNN model to a synthetic validation dataset with low-angle faults. Nonetheless, like a supervised learning approach, such as predicting faults with a CNN trained on synthetic fault dataset, the interpreter carries out the work with a given tectonic model in mind, which highlights the substantial degree of subjectivity and prior assumptions involved in manual seismic interpretation (Bond *et al.* 2012).

Different procedures exist that exploits a trained model and alter its learning towards a similar problem. A great number of fault attributes could be used in comparison to the CNN model results, but we chose some familiar structural attributes, namely variance (Marfurt *et al*. 1998) and ant-tracking (Pedersen *et al*. 2002). Other studies have utilised seismic attributes to guide fault modelling using supervised learning. Di *et al*. (2017) demonstrated how fault detection based on multi-attribute support vector machine classification and guided by manual interpretations could map faults in a 3D seismic cube. Such an approach could be implemented in a CNN model workflow, but the computational cost would be of concern due to the large increase of input data. In terms of using manual interpretations, Wrona *et al*. (2020) and An *et al*. (2021) demonstrated how manually labelled data could be used for fault predictions as mentioned in the introduction section. With regards to the challenge with limited seismic data quality, Cunha *et al*. (2020) demonstrated how transfer learning from a pre-trained neural network could utilise the learning obtained from synthetic seismic data into real data that significantly improved the overall scoring metrics for the fault predictions. Using transfer learning could potentially improve the fault mapping quality of the investigated area in this study.

The CNN model has provided new fault details in the Valdemar Field that may serve as an important input into building a robust static model or flow model. Moreover, due to the probability feature, the CNN model fault predictions are easier to interpret than the variance and ant-tracking attributes. The observed disagreements between the geometries of the fault systems in the CNN results and the manual interpretation shown in the vertical sections motivate for a re-interpretation of structural features occurring within the Cretaceous succession in Valdemar Field at a finer scale. Here, the CNN model predicts faults that are generally planar to slightly curved in nature, which suggests that the faults were deformed after their initial formation. These predictions could be erroneous due to the bias of steep faults in the training data and seismic noise, but the variance and ant-tracking attributes are to some extent in accordance with the CNN proposed fault patterns. Therefore, the CNN model should be treated as an additional fault interpretation tool for the interpreter to quality check in a critical manner. Identifying overlooked faults or adjusting previously interpreted faults may impact the fault mechanism that could influence the fluid migration in the Cretaceous succession (Smit *et al*. 2018). With decreasing commercial hydrocarbon exploration and production activities from the DCG, the proposed supervised learning approach to fault mapping and the results from this work can serve a purpose for prospect evaluation studies of exploiting the chalk fields for geological CO_2 storage (Frykman *et al*. 2009; Suicmez, 2019; Bonto *et al*. 2021).

Conclusion

A pre-trained convolution neural network is applied to the Cretaceous succession in the Valdemar Field, Danish North Sea, for improved fault predictions. The predicted faults show good consistency with the standard seismic attributes used for fault predictions and a manual interpretation. However, a comparison with the manual interpretations in vertical seismic sections show some fault geometry discrepancies in terms of dip angles and extents. As opposed to the manual interpretation, the neural network method suggest steeper and more curved fault geometries in accordance with the seismic variance and ant-tracking attribute. This sheds new light on the existing structural model and structural geological evolution in parts of the study area. The steeper dip angles proposed by the neural network could however be an artefact from the training data being composed of high-dipping planar faults. Moreover, like regular seismic attributes, the neural network is sensitive to seismic noise, which may distort the fault predictions. Hence, the method should be treated as an additional interpretation tool that needs quality checking. The method can yield valuable implications in reservoir characterisation and cap-rock integrity assessments for hydrocarbon exploration and CO_2 storage site evaluations.

Acknowledgements

This research has received funding from the Danish Offshore Technology Centre (DTU Offshore) under the Improved recovery from the tight Lower Cretaceous reservoir (LOCRETA) programme and is part of the PhD project of ML and THH. The authors kindly

acknowledge the Danish Underground Consortium (TotalEnergies E&P Denmark, Noreco and Nordsøfonden) for providing data and granting the permission to publish this work. The authors would like to thank the Software Underground community (SWUNG) for inspiring discussions regarding the machine learning aspect of the study. THH thanks Eliis for generously providing an academic license for the interpretation software, Paleoscan, which was used for the manual fault interpretation. Special thanks should be given to Shahjahan Laghari for the valuable technical support that greatly improved the quality of the study. Lastly, the authors would like to thank the reviewers for their thoughtful comments and efforts towards improving the manuscript.

References

An, Y., Guo, J., Ye, Q., Childs, C., Walsh, J., & Dong, R. 2021: Deep convolutional neural network for automatic fault recognition from 3D seismic datasets. Computers & Geosciences 153, 104776, doi:10.1016/j.cageo.2021.104776.

Araya-Polo, M., Dahlke, T., Frogner, C., Zhang, C., Poggio, T. & Hohl, D. 2017: Automated fault detection without seismic processing. Leading Edge 36, 208–214, doi:10.1190/tle36030208.1.

Bond, C. E., Lunn, R. J., Shipton, Z. K. & Lunn, A. D. 2012: What makes an expert effective at interpreting seismic images? Geology 40, 75–78, doi:10.1130/G32375.1.

Bonto, M. *et al*. 2021: Challenges and enablers for large-scale CO2 storage in chalk formations. EarthScience Reviews 222, 103826, doi:10.1016/j.earscirev.2021.103826.

Bormann P., Aursand P., Dilib F., Dischington P. & Manral S. 2020: FORCE Machine Learning Competition, url:https://github.com/bolgebrygg/ Force-2020-Machine-Learning-competition/.

Bredesen, K., Lorentzen, M., Nielsen, L. & Mosegaard, K. 2021: Quantitative seismic interpretation of the Lower Cretaceous reservoirs in the Valdemar Field, Danish North Sea. Petroleum Geoscience 27, petgeo2021-016, doi:10.1144/petgeo2021-016.

Chopra, S. & Marfurt, K. J. 2007: Seismic attributes for prospect identification and reservoir characterization, 1st edition, 457 pp. Society of Exploration Geophysicists and European Association of Geoscientists and Engineers.

Cunha, A., Pochet, A., Lopes, H. & Gattass, M. 2020: Seismic fault detection in real data using transfer learning from a convolutional neural network pretrained with synthetic seismic data. Computers and Geosciences 135, 104344, doi:10.1016/j.cageo.2019.104344.

Di, H., Shafiq, M. A. & AlRegib, G. 2017: Seismic-fault detection based on multiattribute support vector machine analysis. In 2017 SEG International Exposition and Annual Meeting. OnePetro, 2039–2044, doi:10.1190/segam2017-17748277.1.

Dou, Y., Li, K., Zhu, J., Li, T., Tan, S. & Huang, Z. 2021: Efficient Training of 3D Seismic Image Fault Segmentation Network under Sparse Labels by Weakening Anomaly Annotation, arXiv, doi: 10.48550/arXiv.2110.05319.

Dramsch, J. S. 2020: 70 Years of Machine Learning in Geoscience in Review. Advances in Geophysics 61, 1–55, doi:10.1016/bs.agph.2020.08.002.

Fossen, H. 2016: Structural Geology, 2nd edition, 524 pp., Cambridge University Press, doi:10.1017/9781107415096.

Frykman, P., Bech, N., Sørensen, A. T., Nielsen, L. H., Nielsen, C. M., Kristensen, L. & Bidstrup, T. 2009: Geological modeling and dynamic flow analysis as initial site investigation for large-scale CO2 injection at the Vedsted structure, NW Denmark. Energy Procedia 1, 2975–2982, doi:10.1016/j.egypro.2009.02.074.

Hansen, T. H., Clausen, O. R. & Andresen, K. J. 2021: Thick-and thin-skinned basin inversion in the Danish Central Graben, North Sea-the role of deep evaporites and basement kinematics. Solid Earth 12, 1719–1747, doi:10.5194/se-12-1719-2021.

Ineson, J. R. 1993: The Lower Cretaceous chalk play in the Danish Central trough. Petroleum Geology Conference Proceedings, 4. Geological Society of London, 175–183, doi:10.1144/0040175.

Ineson, J. R., Bojesen-Koefoed, J. A., Dybkjær, K. & Nielsen, L. H. 2003: Volgian-Ryazanian 'hot shales' of the Bo Member (Farsund Formation) in the Danish Central Graben, North Sea: Stratigraphy, facies and geochemistry. Geological Survey of Denmark and Greenland Bulletin 1, 403–436, doi:10.34194/geusb.v1.4679.

Jakobsen, F., Ineson, J. R., Kristensen, L. & Stemmerik, L. 2004: Characterization and zonation of a marly chalk reservoir: The Lower Cretaceous Valdemar field of the Danish Central Graben. Petroleum Geoscience 10, 21–33, doi:10.1144/1354-079303-584.

Jakobsen, F., Ineson, J. R., Kristensen, L., Nytoft, H. P. & Stemmerik, L. 2005: The Valdemar field, Danish central graben: Field compartmentalization and regional prospectivity of the Lower Cretaceous chalk play. In Petroleum Geology Conference Proceedings, 6. Geological Society of London, 177–186, doi:10.1144/0060177.

Long, J., Shelhamer, E. & Darrell, T. 2015: Fully Convolutional Networks for Semantic Segmentation. 2015 IEEE Conference on Computer Vision and Pattern Recognition, 3431–3440, doi: 10.1109/CVPR.2015.7298965.

Madsen, L. & Britze, P. 1999: PRIORITY - Improved oil recovery and productivity from Lower Cretaceous Carbonates – EFP-97. Sub-project 1.4.a: Seismic interpretation of the Cretaceous in the Valdemar Area. The Geological Survey of Denmark and Greenland.

Marfurt, K. J., Sudhakar, V., Gersztenkorn, A., Crawford, K. D. & Nissen, S. E. 1997: Coherency calculations in the presence of structural dip. 1997 SEG Annual Meeting 64, 566–569, doi:10.1190/1.1885964.

Marfurt, K. J., Kirlin, R. L., Farmer, S. L. & Bahorich, M. S. 1998:

3-D seismic attributes using a semblance-based coherency algorithm. Geophysics 63, 1150–1165, doi:10.1190/1.1444415.

Møller, J. J. & Rasmussen, E. S. 2003: Middle Jurassic–Early Cretaceous rifting of the Danish Central Graben. Geological Survey of Denmark and Greenland Bulletin 1, 247–264, doi:10.34194/geusb.v1.4654.

Montazeri, M., Uldall, A., Moreau, J. & Nielsen, L. 2018: Pitfalls in velocity analysis for strongly contrasting, layered media – Example from the Chalk Group, North Sea. Journal of Applied Geophysics 149, 52–62, doi:10.1016/j.jappgeo.2017.12.003.

Pedersen, S. I., Randen, T., Sønneland, L. & Steen, Ø. 2002: Automatic fault extraction using artificial ants. In SEG Technical Program Expanded Abstracts. Society of Exploration Geophysicists 21, 512–515, doi:10.1190/1.1817297.

Randen, T., Pedersen, S. I. & Sønneland, L. 2001: Automatic extraction of fault surfaces from three-dimensional seismic data. 2001 SEG Annual Meeting. Society of Exploration Geophysicists, 551–554, doi:10.1190/1.1816675.

Ronneberger, O., Fischer, P., & Brox, T. 2015: U-net: Convolutional networks for biomedical image segmentation. International Conference on Medical image computing and computer-assisted intervention 9351, 234-241, doi:10.1007/978-3-319-24574-4_28.

Smit, F. W., van Buchem, F. S. , Holst, J. C., Lüthje, M., Anderskouv, K., Thibault, N., Buijs, G. J., Welch, M. J. & Stemmerik, L. 2018: Seismic geomorphology and origin of diagenetic geobodies in the Upper Cretaceous Chalk of the North Sea Basin (Danish Central Graben). Basin Research 30, 895–925, doi:10.1111/bre.12285.

Smit, F. W., Stemmerik, L., Lüthje, M. & van Buchem, F. S. 2021: Characterization and origin of large Campanian depressions within the Chalk Group of the Danish Central Graben – implications for hydrocarbon exploration and development. Geological Society Special Publication 509, 249–282, doi:10.1144/SP509-2019-126.

Sorkhabi, R. & Tsuji, Y. 2005: Faults, Fluid Flow, and Petroleum Traps. Faults, Fluid Flow, and Petroleum Traps, 1st edition, 343 pp. American Association of Petroleum Geologists Memoir 85, doi:10.1306/m851033.

Suicmez, V. S. 2019: Feasibility study for carbon capture utilization and storage (CCUS) in the Danish North Sea. Journal of Natural Gas Science and Engineering 68, 102924, doi:10.1016/j.jngse.2019.102924.

van Bemmel, P. & Pepper, R. E. F. 2000: Seismic signal processing and apparatus for generating a cube of variance values. U.S. Patent 6151555.

van Buchem, F. S., Smit, F. W., Buijs, G. J., Trudgill, B. & Larsen, P. H. 2018: Tectonostratigraphic framework and depositional history of the Cretaceous-Danian succession of the Danish Central Graben (North Sea) - new light on a mature area. In Petroleum Geology Conference Proceedings, 8. Geological Society of London, 9–46, doi:10.1144/PGC8.24.

Vejbæk, O. V. 1986: Seismic stratigraphy and tectonic evolution of the Lower Cretaceous in the Danish Central Trough, Danmarks Geologiske Undersøgelse Serie A 11, 1-46, doi:10.34194/seriea.v11.7030.

Vejbæk, O. V. & Andersen, C. 2002: Post mid-Cretaceous inversion tectonics in the Danish Central Graben - regionally synchronous tectonic events? Bulletin of the Geological Society of Denmark 49, 129–144, doi:10.37570/bgsd-2003-49-11.

Vidalie, M., van Buchem, F., Schmidt, I. & Uldall, A. 2012: Seismic stratigraphy of the Lower Cretaceous Valhall Formation, Danish Graben, North Sea. 74th European Association of Geoscientists and Engineers Conference and Exhibition, 5327–5331, doi:10.3997/2214-4609.20148747.

Wrona, T., Pan, I., Bell, R. E., Gawthorpe, R. L., Fossen, H. & Brune, S. 2020: Deep learning of geological structures in seismic reflection data. Geophysics (submitted), doi: 10.31223/X5S88B.

Wu, X. & Hale, D. 2016: 3D seismic image processing for faults. Geophysics 81, IM1– IM11, doi:10.1190/GEO2015-0380.1.

Wu, X., Liang, L., Shi, Y. & Fomel, S. 2019: FaultSeg3D: Using synthetic data sets to train an end-to-end convolutional neural network for 3D seismic fault segmentation. Geophysics 84, IM35–IM45, doi:10.1190/geo2018-0646.1.

Ziegler, P. 1990: Geological Atlas of Western and Central Europe, Shell Internationale Petroleum Maatschappij B.V., the Hauge, 238 pp.